Supporting Information for

Highly Li^+-conductive $HfNb_{24}O_{62}$ anode material for superior Li^+ storage

Experimental section

Material preparation

$HfNb_{24}O_{62}$ was prepared through a one-step solid-state reaction procedure. Briefly, HfO_2 (Aladdin, 99.99%) and Nb_2O_5 (Aladdin, 99.5%) powders with a molar ratio of 1 : 12 were ball-milled for 1 h using a SPEX-8000M ball apparatus, and then heated to 1250 °C for 4 h in a box furnace with a ramp of 10 °C min^{-1} to obtain the pale yellowish $HfNb_{24}O_{62}$ powders.

Material characterization

The powder X-ray diffraction (XRD) test was performed on a Brucker D8 advance diffractometer. The Rietveld refinement was performed using the GSAS software with the EXPGUI interface [S1,S2]. The X-ray photoelectron spectroscopy (XPS) test was performed using a Thermo Escalab 250Xi photoelectron spectrometer. The particle size, morphology and

microstructure were characterized by field-emission scanning electron microscopy (FESEM, Hitachi S-4800, Japan) and high-resolution transmission electron microscopy (HRTEM, FEI Tecnai G2 F20 STWIN, USA). The specific surface area was analyzed using the Branauer–Emmett–Teller (BET) theory with a porosity and surface area analyzer (ASAP 2020, USA).

Electrochemical test

The working electrode was fabricated by blending the $HfNb_{24}O_{62}$ powder, conductive carbon (Super P®), and polyvinylidene fluoride (PVDF) at a weight ratio of 65:25:10 in an N-methylpyrrolidinone (NMP) solvent. The formed slurry was uniformly spread on Cu current collectors followed by vacuum drying at 120 °C for 4 h. CR2016-type coin cells were assembled in an Ar-filled glove box. $HfNb_{24}O_{62}$ on Cu current collectors, lithium metal foils, and Celgard 2325® microporous polypropylene films were used as the working electrodes, counter electrodes, and separators, respectively. The electrolyte was 1 M $LiPF_6$ in a mixture of ethylene carbonate (EC), dimethyl carbonate (DMC), and diethylene carbonate (DEC) at a volume ratio of 1:1:1.

Galvanostatic discharging/charging tests and galvanostatic intermittent titration technique (GITT) experiments were performed on an automatic battery testing system (CT-3008, Neware) in a potential range of 0.8–3.0 V. Here, 378 mA g^{-1} is equivalent to 1C, as calculated from the theoretical capacity of $HfNb_{24}O_{62}$ (378 mAh g^{-1}). Cyclic voltammetry (CV) curves were collected *via* an electrochemical workstation (CHI660E, China).

Detailed process of Rietveld refinement

Since this is the first fabrication of $HfNb_{24}O_{62}$, no existing crystal data for $HfNb_{24}O_{62}$ can be found in previous reports. However, on the basis of the known crystal data of $TiNb_{24}O_{62}$, the detailed crystal structure of $HfNb_{24}O_{62}$ was successfully clarified through a Rietveld refinement. First, the "cif" (Crystallographic Information File) file of $TiNb_{24}O_{62}$ was imported into the GSAS program. Second, in the program, "Ti" was changed to "Hf", and the site occupancies of Hf and Nb were set to be 0.04 and 0.96, respectively. Third, two files respectively containing the instrumental parameters and experimental diffraction data were imported into the program. Finally, the following instrumental and structural parameters were successively refined: background parameters, zero-shift, unit-cell parameters, profile parameters, atomic fractional coordinates, and atomic isotropic displacement parameters. All isotropic temperature factors were fixed to be the same. The site occupancies were assumed to fulfill the stoichiometric composition of $HfNb_{24}O_{62}$. The site occupancy of oxygen atoms was fixed to be unity.

Calculation of Li^+ diffusion coefficient through GITT

GITT with a current pulse at 0.1 C for 10 min between rest intervals of 20 min was applied to elucidate the Li^+ diffusion coefficient (D_{Li}) of $HfNb_{24}O_{62}$ during the initial two cycles. The D_{Li} value can be estimated according to Fick's second law following **Eq. (S1)** [S3]:

$$D_{Li} = \frac{4}{\pi}\left(\frac{m_B V_m}{M_B S}\right)^2 \left(\frac{\Delta E_s}{\tau\left(dE_\tau / d\sqrt{\tau}\right)}\right)^2 \qquad \left(\tau \ll \frac{L^2}{D_{Li}}\right) \tag{S1}$$

where m_B (g) and M_B (g mol^{-1}) are the mass and molar weight of $HfNb_{24}O_{62}$, S (cm^2) is the real surface area of $HfNb_{24}O_{62}$ based on its BET specific surface area, τ (s) is the rest time, and ΔE_s (V) and ΔE_τ (V) represent the equilibrium potential change and current pulse potential change, respectively (**Fig. S6a**). Since ΔE_τ is linearly proportional to $\tau^{0.5}$ (**Fig. S6b**), **Eq. (S1)** can be further simplified to **Eq. (S2)**:

$$D_{Li} = \frac{4}{\pi\tau}\left(\frac{m_B V_m}{M_B S}\right)^2\left(\frac{\Delta E_s}{\Delta E_\tau}\right)^2 \qquad \left(\tau \ll \frac{L^2}{D_{Li}}\right) \tag{S2}$$

Based on the calculation, the evolving D_{Li} of $HfNb_{24}O_{62}$ at each potential in the discharging (lithiation) and charging (delithiation) processes is plotted in **Fig. 2j**.

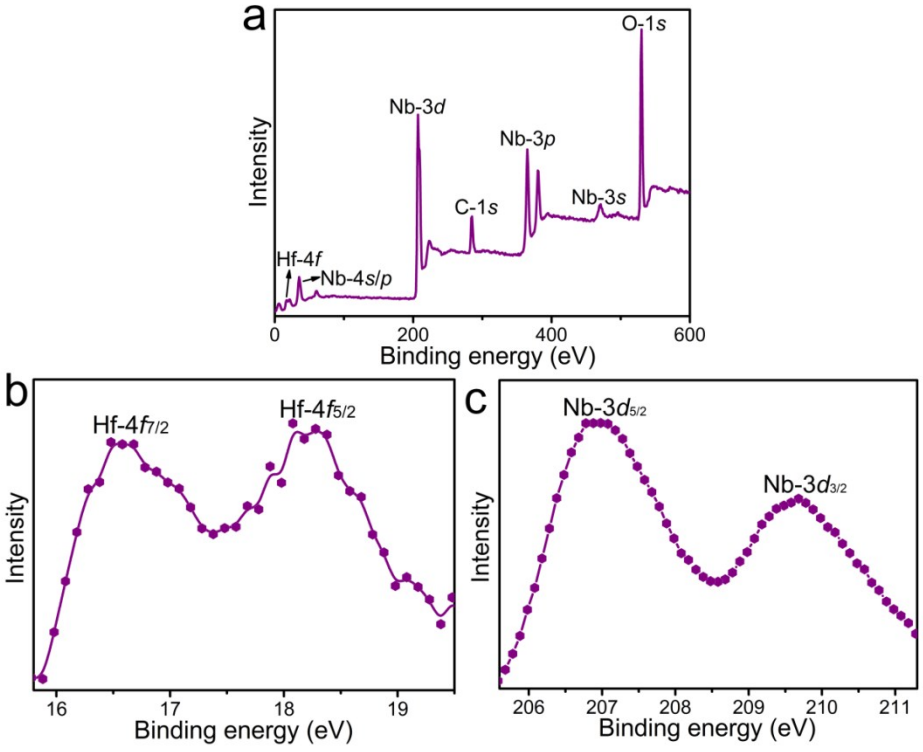

Fig. S1. XPS characterizations: (a) survey spectrum, and detailed spectra of (b) Hf and (c) Nb

elements.

XPS was employed to investigate the valence states of the hafnium and niobium elements in $HfNb_{24}O_{62}$. The survey XPS spectrum reveals the presence of Hf, Nb, O and C (reference) elements (**Fig. S1a**). The Hf-4*f* spectrum (**Fig. S1b**) with two characteristic peaks at 16.6 eV (Hf-$4f_{7/2}$) and 18.3 eV (Hf-$4f_{5/2}$) indicates hafnium in the tetravalent state (Hf^{4+}) [S4]. The peaks at 206.9 and 209.7 eV (**Fig. S1c**) can be ascribed to Nb-$3d_{5/2}$ and Nb-$3d_{3/2}$, indicating the pentavalent niobium ions (Nb^{5+}) in $HfNb_{24}O_{62}$ [S5].

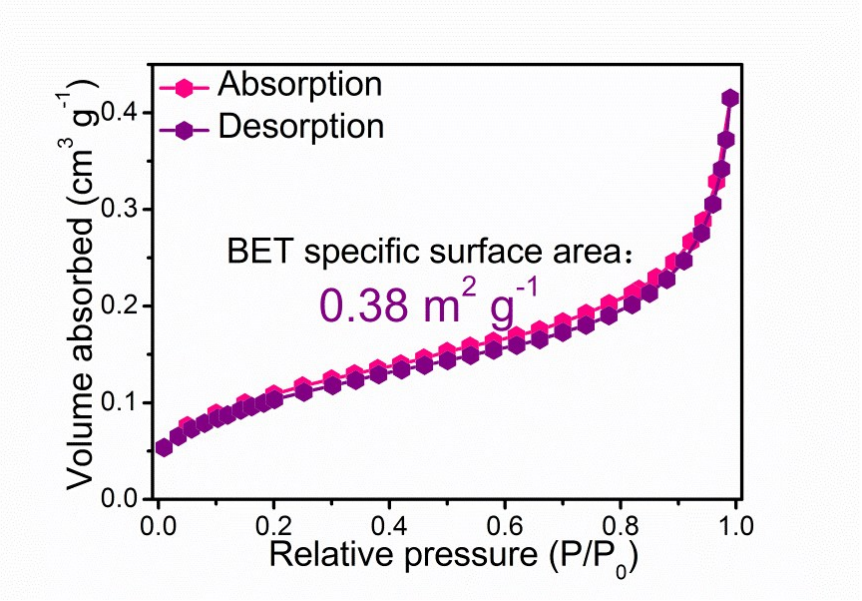

Fig. S2. N_2 adsorption/desorption isotherm of $HfNb_{24}O_{62}$.

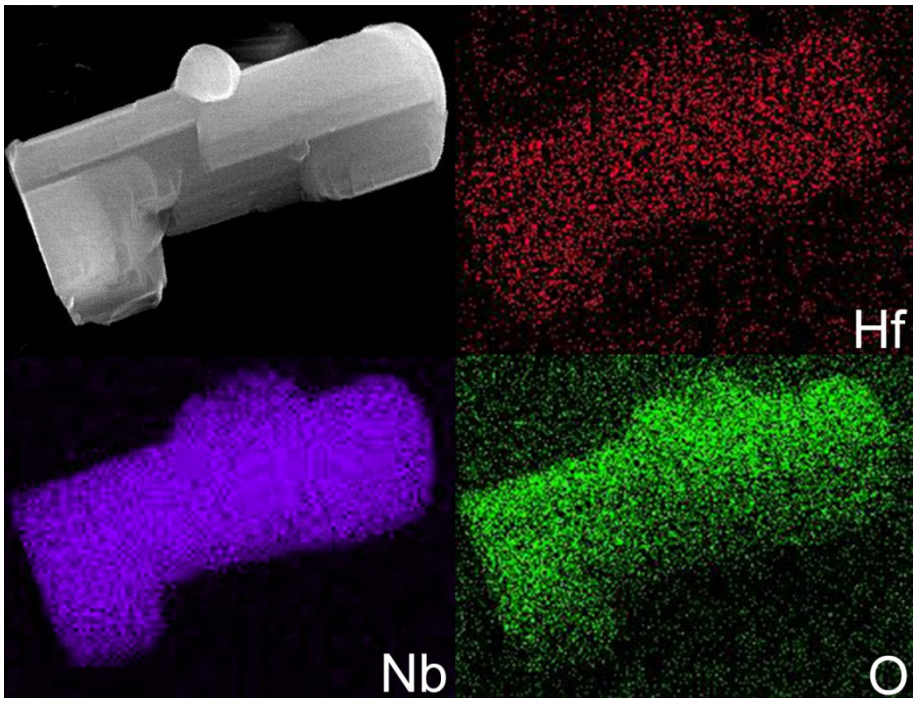

Fig. S3. EDX elemental mapping images of $HfNb_{24}O_{62}$.

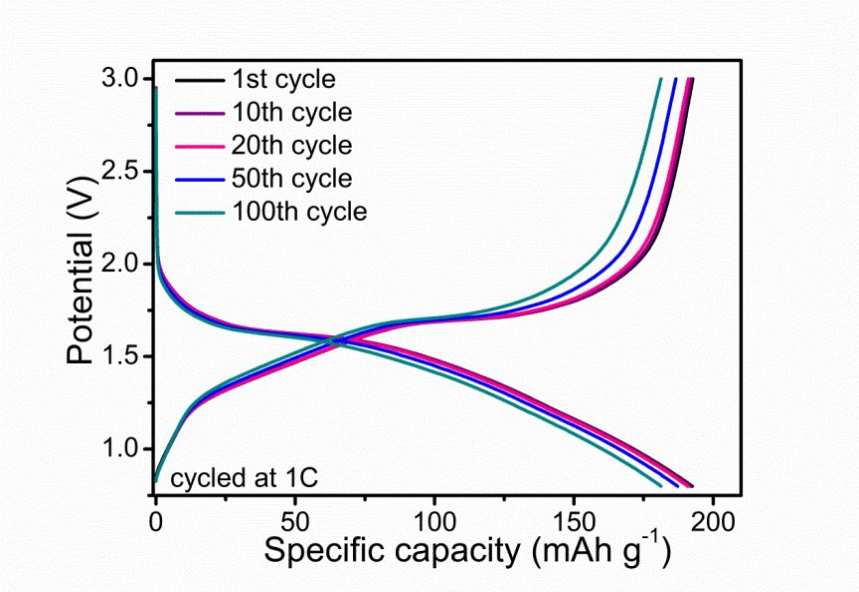

Fig. S4. Discharging/charging curves of $HfNb_{24}O_{62}$/Li cell in different cycles at 1 C.

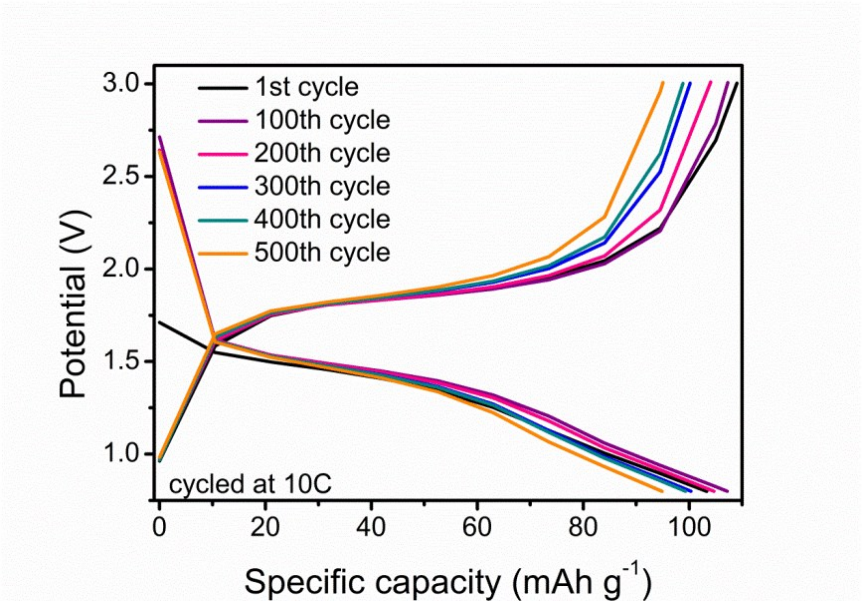

Fig. S5. Discharging/charging curves of $HfNb_{24}O_{62}$/Li cell in different cycles at 10 C.

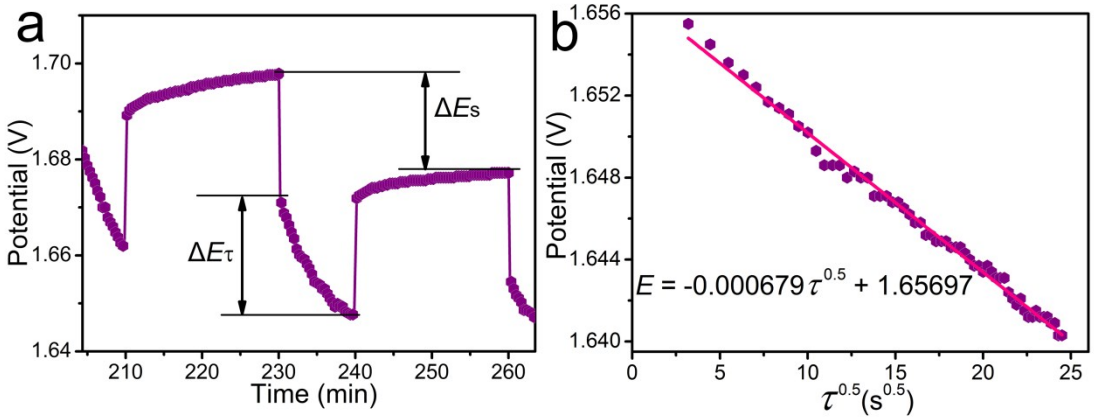

Fig. S6. (a) Polarization curve of single GITT discharge process, and (b) relationship between E and $\tau^{0.5}$ for $HfNb_{24}O_{62}$/Li cell.

Table S1. Fractional atomic parameters of $HfNb_{24}O_{62}$ (space group of *C2*).

atom*	symmetry	site	*x*	*y*	*z*
M1	2	2*a*	0	0.25	0
M2	1	4*c*	0.1159	0	0.0093
M3	1	4*c*	0.2407	0	0.0593
M4	1	4*c*	0.3671	0	0.1121
M5	1	4*c*	0.5007	0	0.1644
M6	1	4*c*	0.0904	0	0.1837
M7	1	4*c*	0.2249	0	0.2363
M8	1	4*c*	0.3507	0	0.2884
M9	1	4*c*	0.4727	0	0.3368
M10	1	4*c*	0.0715	0	0.3638
M11	1	4*c*	0.1957	0	0.4117
M12	1	4*c*	0.3207	0	0.4628
M13	1	4*c*	0.4484	0	0.5102
O1	1	4*c*	0.3779	0	0.0110
O2	1	4*c*	0.1746	0	0.0341
O3	1	4*c*	0.3196	0	0.0838
O4	1	4*c*	0.0996	0	0.1030
O5	1	4*c*	0.4340	0	0.1377
O6	1	4*c*	0.2214	0	0.1492
O7	1	4*c*	0.0157	0	0.1428
O8	1	4*c*	0.3787	0	0.1919
O9	1	4*c*	0.1432	0	0.2123
O10	1	4*c*	0.4830	0	0.2531
O11	1	4*c*	0.2794	0	0.2658
O12	1	4*c*	0.0700	0	0.2828
O13	1	4*c*	0.4152	0	0.3066
O14	1	4*c*	0.2116	0	0.3433
O15	1	4*c*	0.3247	0	0.3872
O16	1	4*c*	0.1278	0	0.3908
O17	1	4*c*	0.4770	0	0.4479
O18	1	4*c*	0.2634	0	0.4385
O19	1	4*c*	0.0455	0	0.4866
O20	1	4*c*	0.3927	0	0.5009
O21	1	4*c*	0.1780	0	0.4995
O22	1	4*c*	0.3160	0	0.5577
O23	1	4*c*	0.4363	0	0.6311
O24	1	4*c*	0.0109	0	0.6607
O25	1	4*c*	0.1294	0	0.7161

O26	1	4*c*	0.2768	0	0.7829
O27	1	4*c*	0.4211	0	0.8355
O28	1	4*c*	0.1342	0	0.9036
O29	1	4*c*	0.4847	0	0.9298
O30	1	4*c*	0.2514	0	0.9554
O31	1	4*c*	0.0405	0	0.9852

*M = $0.04Hf^{4+} + 0.96Nb^{5+}$

Table S2. Comparisons of Li^+ diffusion coefficient (D_{Li}) of $HfNb_{24}O_{62}$ with other niobium-based oxide anode materials.

material	D_{Li} ($cm^2\ s^{-1}$)	test technique	reference
$HfNb_{24}O_{62}$	$1.6\sim1.7\times10^{-12}$	GITT	this work
Ti-Nb oxide composite microspheres	3.47×10^{-15}	CV	[S6]
$GeNb_{18}O_{47}$ nanowires	1.552×10^{-14}	CV	[S7]
$TiNb_6O_{17}$	4.28×10^{-14}	CV	[S8]
$Ti_2Nb_{10}O_{27.1}$	1.84×10^{-14}	CV	[S9]
$Cu_{0.02}Ti_{0.94}Nb_{2.04}O_7$	1.66×10^{-14}	EIS	[S10]
$Ru_{0.01}Ti_{0.99}Nb_2O_7$	1.66×10^{-15}	EIS	[S11]
$TiNb_2O_7$ nanorods	3.39×10^{-14}	CV	[S12]
$TiNb_2O_7$/CNTs nanocomposite	9.27×10^{-16}	CV	[S13]
$TiNb_2O_7$ mesoporous microspheres	3.34×10^{-15}	EIS	[S14]
$TiCr_{0.5}Nb_{10.5}O_{29}$	2.09×10^{-14}	CV	[S15]
$Cr_{0.5}Nb_{24.5}O_{62}$	4.57×10^{-14}	EIS	[S16]
VNb_9O_{25} nanoribbons	5.17×10^{-15}	EIS	[S17]

References

[S1]B.H. Toby, EXPGUI, a graphical user interface for GSAS, J. Appl. Crystallogr. 34 (2001) 210–213.

[S2]A.C. Larson, R.B. Von Dreele, General structure analysis system (GSAS), Los Alamos National Laboratory Report LAUR 86–748, 1994.

[S3]W. Weppner, R.A. Huggins, Determination of the kinetic parameters of mixed-conducting electrodes and application to the system Li_3Sb, J. Electrochem. Soc. 124 (1977) 1569–1578.

[S4]A.N. Mansour, Nickel monochromated Al Kα XPS spectra from the physical electronics model 5400 spectrometer, Surf. Sci. Spectra 3 (1994**)** 221–230.

[S5]L. Hu, L.J. Luo, C.F. Lin, R.J. Li, Y.J. Chen, $Ti_2Nb_{2x}O_{4+5x}$ anode materials for lithium-ion batteries: a comprehensive review, J. Mater. Chem. A 6 (2018) 9799–9815.

[S6]G.Q. Wang, Z.S. Wen, L.L. Du, Y.E. Yang, S. Li, J.C. Sun, S.J. Ji, Hierarchical Ti-Nb oxide microspheres with synergic multiphase structure as ultra-long-life anode materials for lithium-ion batteries, J. Power Sources 367 (2017) 106–115.

[S7]F.M. Ran, X. Cheng, H.X. Yu, R.T. Zheng, T.T. Liu, X.F. Li, N. Ren, M. Shui, J. Shu, Nano-structured $GeNb_{18}O_{47}$ as novel anode host with superior lithium storage performance, Electrochim. Acta 282 (2018) 634–641.

[S8]C.F. Lin, G.Z. Wang, S.W. Lin, J.B. Li, L. Lu, $TiNb_6O_{17}$: a new electrode material for lithium-ion batteries, Chem. Commun. 51 (2015) 8970–8973.

[S9]C.F. Lin, S. Yu, H. Zhao, S.Q. Wu, G.Z. Wang, L. Yu, Y.F. Li, Z.Z. Zhu, J.B. Li, S.W. Lin, Defective $Ti_2Nb_{10}O_{27.1}$: an advanced anode material for lithium-ion batteries, Sci. Rep. 5 (2015) 17836.

[S10]C. Yang, C.F. Lin, S.W. Lin, Y.J. Chen, J.B. Li, $Cu_{0.02}Ti_{0.94}Nb_{2.04}O_7$: an advanced anode material for lithium-ion batteries of electric vehicles, J. Power Sources 328 (2016) 336–344.

[S11]C.F. Lin, S. Yu, S.Q. Wu, S.W. Lin, Z.Z. Zhu, J.B. Li, L. Lu, $Ru_{0.01}Ti_{0.99}Nb_2O_7$ as an intercalation-type anode material with a large capacity and high rate performance for lithium-ion batteries, J. Mater. Chem. A 3 (2015) 8627–8635.

[S12]L. Hu, C.F. Lin, C.H. Wang, C. Yang, J.B. Li, Y.J. Chen, S.W. Lin, $TiNb_2O_7$ nanorods as a novel anode material for secondary lithium-ion batteries, Funct. Mater. Lett. 9 (2016) 1642004.

[S13]C.F. Lin, L. Hu, C.B. Cheng, K. Sun, X.K. Guo, Q. Shao, J.B Li, N. Wang, Z.H. Guo, Nano-$TiNb_2O_7$/carbon nanotubes composite anode for enhanced lithium-ion batteries of electric vehicles, Electrochim. Acta 260 (2018) 65–72.

[S14]G.Y. Liu, L.F. Zhao, R.X. Sun, W.H. Chen, M. Hu, M. Liu, X.Y. Duan, T.M. Zhang, Mesoporous $TiNb_2O_7$ microspheres as high performance anode materials for lithium-ion batteries with high-rate capability and long cycle-life, Electrochim. Acta 259 (2018) 20–27.

[S15]L. Hu, R.H. Lu, L.F. Tang, R. Xia, C.F. Lin, Z.B. Luo, Y.J. Chen, J.B. Li, $TiCr_{0.5}Nb_{10.5}O_{29}$/CNTs nanocomposite as an advanced anode material for high-performance Li^+-ion storage, J. Alloys Compd. 732 (2018) 116–123.

[S16]C. Yang, S. Yu, C.F. Lin, F. Lv, S.Q. Wu, Y. Yang, W. Wang, Z.Z. Zhu, J.B. Li, N. Wang, S.J. Guo, $Cr_{0.5}Nb_{24.5}O_{62}$ nanowires with high electronic conductivity for high-rate and long-life lithium-ion storage, ACS Nano 11 (2017) 4217–4224.

[S17]S.S. Qian, H.X. Yu, L. Yan, H.J. Zhu, X. Cheng, Y. Xie, N.B. Long, M. Shui, J. Shu, High-rate long-life pored nano-ribbon VNb_9O_{25} built by interconnected ultrafine nanoparticles as anode for lithium-ion batteries, ACS Appl. Mater. Interfaces 9 (2017) 30608–30616.